ADVANCED ENERGY MATERIALS
www.advenergymat.de

Advanced Extremely Durable 3D Bifunctional Air Electrodes for Rechargeable Zinc-Air Batteries

*Dong Un Lee, Ja-Yeon Choi, Kun Feng, Hey Woong Park, and Zhongwei Chen**

With the emergence of electric and hybrid electric vehicles, advanced energy generation and storage systems have become one of the focal points of scientific research. Metal-air battery technologies such as zinc-air and lithium-air batteries offer extremely high theoretical energy capacities, making them excellent candidates as range extenders for these next generation vehicles.[1–6] Zinc-air batteries, in particular, are affordable, safe, and environmentally benign, making them ideally suited for a wide range of applications. However, for rechargeable battery applications one of the main challenges associated with the commercialization of zinc-air batteries is the development of electrocatalysts with high bifunctionality in order to efficiently catalyze both the oxygen reduction reaction (ORR) and oxygen evolution reaction (OER).[2,7,8] To date, efficient ORR and OER processes, which correspond to discharge and charge reactions of a rechargeable zinc-air battery, have been realized using precious metal-based catalysts such as carbon-supported platinum and iridium.[9–12] However, the scarcity and electrochemical instability of these catalysts have prevented the realization of wide commercialization due to extremely high costs and lack of long term durability.[13,14]

The conventional preparation of air-breathing cathodes for zinc-air batteries requires physical deposition of an active material onto a carbon gas diffusion layer (GDL) by methods such as drop-casting or spray-coating.[2,7,15] These physical processes, however, require the use of ancillary materials such as carbon black, pore forming agents, and polymer binders, which often have a negative impact on the battery's performance. In particular for rechargeable battery applications, carbon present in the air cathode spontaneously undergoes side reactions such as carbon corrosion during the high potentials associated with recharging of the battery that leads to the degradation of the electrode, greatly reducing the cycle life of a battery.[16,17] To address these issues of the conventional preparation of air electrodes, we have completely removed the use of ancillary materials by directly growing Co_3O_4 nanowire (NW) array as the active material onto the surface of stainless steel (SS) mesh current collector. The direct growth has several advantages over the conventional methods. First, Co_3O_4 NWs directly grown on SS mesh current collector drastically simplifies the electrode design and fabrication procedure because time-consuming physical deposition processes are no longer required, thus allowing highly practical and scalable preparation of the electrode. Second, non-conductive ancillary binding material removed from the electrode enhances the electrical property and improves the electrochemical stability because the decomposition of the binder can be avoided. Lastly, SS mesh acts as support for the growth of Co_3O_4 NWs and plays the role of a current collector, simplifying the battery design thereby significantly reducing its internal resistance. Using this advanced electrode, remarkable rechargeability and durability of a practical zinc-air battery are demonstrated by utilizing natural air as the source of fuel instead of pure purged oxygen.

The facile template-free method is used to grow mesoporous Co_3O_4 NW array directly onto a SS mesh current collector to be used as an air cathode in rechargeable zinc-air batteries without further processing (**Figure 1**a). The bare SS mesh current collector is observed to be densely coated with Co_3O_4 NW after the growth, creating 3D binder-free, and self-standing NW array (Figure 1b,c and Supporting Information Figure S1a,b). Co_3O_4 NWs consist of average diameter and length of 300 nm and 15 μm, respectively, and they exhibit rounded surface modulation and grow in random directions with some wires crossing each other (Figure 1d). The self-standing nature of the NW array increases the active surface area and allows better diffusion of reactants through the empty spaces between the neighboring NWs.[18] Unlike most template-assisted growth of NW arrays, the simple chemical route employed here produces a uniform and dense Co_3O_4 NW array over large areas, which leads to high surface area per unit volume for enhanced electrocatalytic oxygen reactions (Figure 1e). Interestingly, the Co_3O_4 NWs are tubular with a circular hollow center of diameter 50 nm (Figure 1f), which is ascribed to the Kirkendall effect during the formation of the NWs.[19] Inspection of SS mesh edge reveals a NW array directly coupled to the SS current collector (Supporting Information Figure S1c). The coupling allows direct transfer of charges from the site of the electrocatalytic reaction to the current collector, greatly enhancing the charge transfer properties of the electrode.[18] In addition, every NW is able to undergo an efficient electrochemical reaction because they are individually in contact with the current collector, resulting in a high active material utilization.[18,20] Further analysis reveals that the NWs are mesoporous (Figure 1g and Supporting Information Figure S2a,b), which has also been confirmed by BET (Brunauer-Emmett-Teller) analysis by a type IV isotherm (Supporting Information Figure S3). The high-resolution transmission electron microscopy (HR-TEM) image reveals fringes in multiple directions (Figure 1h), and the crystal structure of the NWs analyzed by fast Fourier transformation (FFT)

D. U. Lee, J.-Y. Choi, K. Feng, H. W. Park, Prof. Z. Chen
Department of Chemical Engineering
Waterloo Institute for Nanotechnology
Waterloo Institute for Sustainable Energy
University of Waterloo
200 University Ave. West, Waterloo, ON, Canada, N2L 3G1
E-mail: zhwchen@uwaterloo.ca

DOI: 10.1002/aenm.201301389

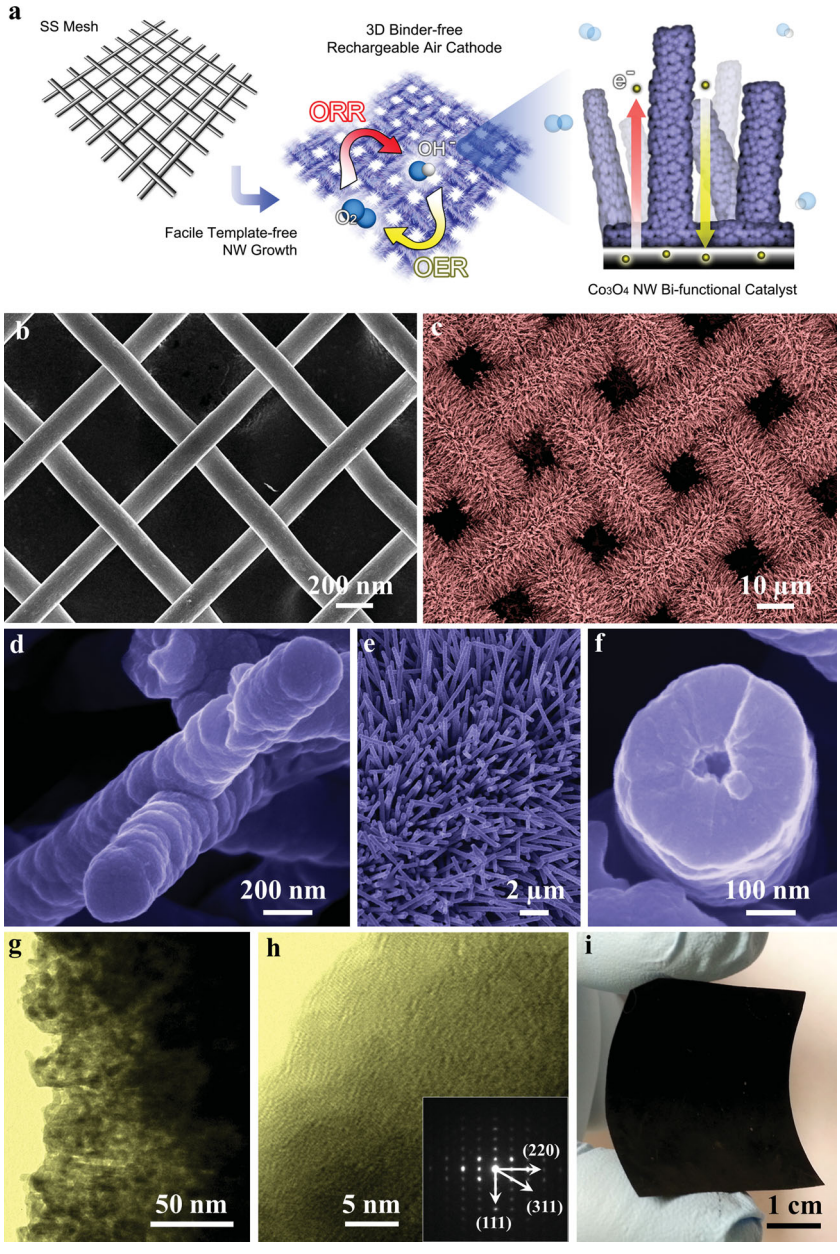

Figure 1. a) Schematic illustration of the growth of 3D rechargeable Co_3O_4 NW air cathode for bifunctional catalysis of ORR and OER. Scanning electron microscopy (SEM) images of b) SS mesh current collector prior to the growth, c) densely coated Co_3O_4 NW array, d) surface morphology of Co_3O_4 NWs, e) self-standing Co_3O_4 NW array, and f) cross-section of Co_3O_4 NWs. g) TEM image of a mesoporous Co_3O_4 NW wall. h) HR-TEM image of the Co_3O_4 NW wall. Inset: FFT pattern of Co_3O_4 NWs exhibiting polycrystallinity. i) Optical image of a flexible, as-grown Co_3O_4 NW air electrode.

reveals (111), (211), and (220) crystal orientations of a cubic spinel Co_3O_4 (Figure 1h, inset), indicative of the polycrystalline nature of the NWs. In addition to the aforementioned advantages, the mechanical flexibility of the SS mesh allows bending of the electrode, which is interesting for the development of flexible device applications (Figure 1i).

To investigate the catalytic activity of the advanced SS mesh electrode, a single-cell practical zinc-air battery was used to demonstrate its performance in natural air (instead of pure oxygen). Superior discharge and charge potentials of the advanced SS mesh electrode are apparent in the galvanodynamic discharge and charge polarization profiles beyond 20 mA cm^{-2} (**Figure 2**a). However, at lower current densities, the conventional GDL electrode sprayed-coated with Co_3O_4 NWs shows a comparable performance to that of the SS mesh electrode due to sufficiently low rate of reaction. The superior performance of the advanced SS mesh electrode at higher current densities is attributed to the hierarchical Co_3O_4 NW array with mesoporous morphology and the direct coupling of each NW onto the current collector for enhanced active material utilization and rapid charge transfer during the catalytic oxygen reactions. In the conventional GDL electrode, however, polymer binders used during the electrode preparation introduce highly undesirable interfaces, which reduce the surface utilization, resulting in inefficient electrocatalysis. Physically deposited material is also subject to particle aggregation, which leads to the loss of active surface area and hindering the accessibility of the electrolyte to the active material.[21] Furthermore, physical deposition leads to random orientations of the active material, which reduces the morphological benefit of the nanosized array architecture. The state-of-art commercial Pt/C catalyst sprayed on a GDL demonstrates comparable discharge performance, but a significantly worse charge performance. The rechargeability of the electrodes has also been tested using air in ambient conditions by the galvanostatic recurrent pulse method with each pulse cycle lasting 10 min (5 min each for discharge/charge) at a fixed current of 50 mA. The pulse cycling technique is an excellent diagnostic tool for evaluating the battery's rechargeability by switching the polarity of applied current in short intervals. The SS mesh electrode with directly grown Co_3O_4 NW array exhibits superior initial charge and discharge potentials of 2.0 and 0.98 V, respectively (Figure 2b). Even after 100 pulse cycles, the discharge and charge potentials remain virtually unchanged, which is indicative of excellent rechargeability. In fact, even after 1500 pulse cycles, the performance of the SS mesh electrode shows only a slight decrease in the discharge potential (Supporting Information Figure S7). In contrast, the conventional Co_3O_4 NW sprayed and Pt/C sprayed GDL electrodes show significant potential losses after 100 and 60 pulse cycles, respectively (Figure 2c,d). The carbon-based GDL and the polymer binder used to prepare the electrodes have most likely undergone deterioration.

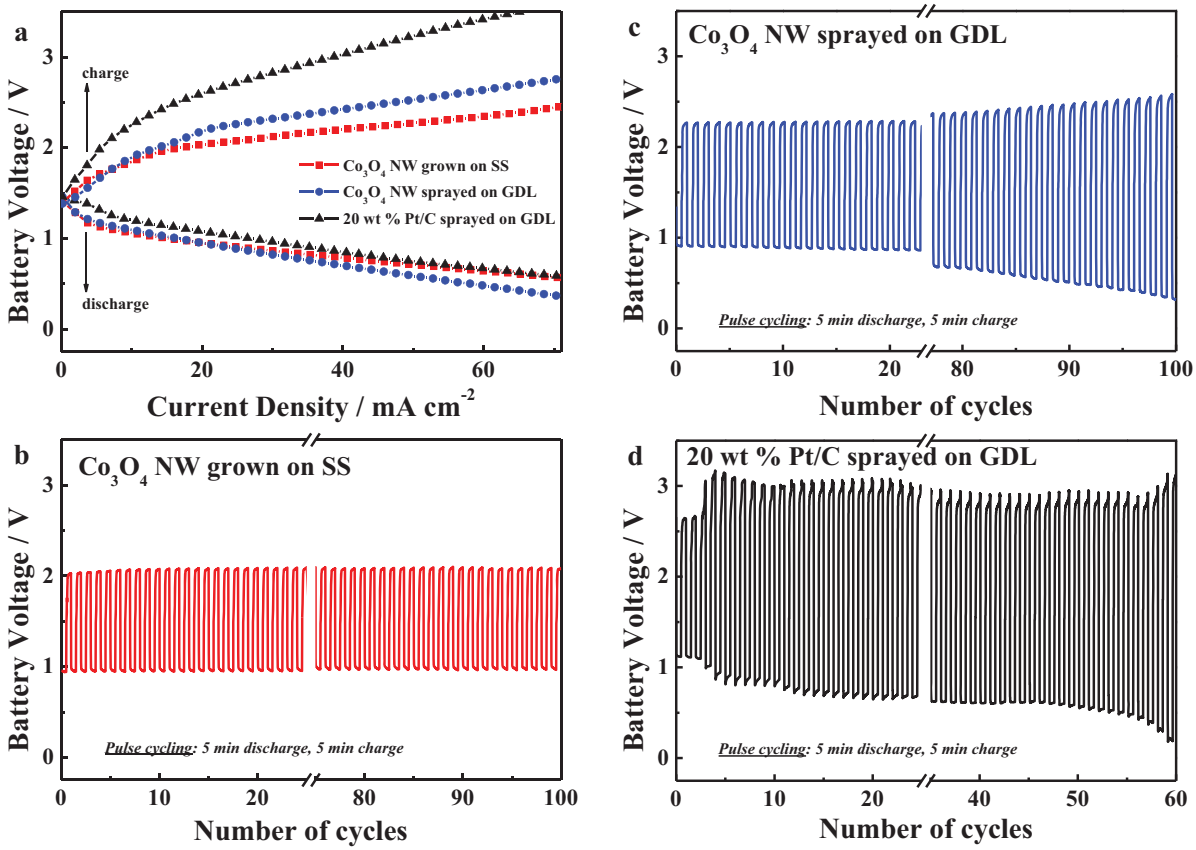

Figure 2. a) Galvanodynamic discharge and charge polarization curves obtained using air under ambient conditions of Co_3O_4 NWs grown on SS mesh (red square), Co_3O_4 NWs sprayed on GDL (blue circle), and Pt/C sprayed on GDL (black triangle). Galvanostatic pulse cycling at 50 mA using air in ambient conditions of b) Co_3O_4 NWs grown on SS mesh, c) Co_3O_4 NWs sprayed on GDL, and d) Pt/C sprayed on GDL.

The evaluation of the enhanced electrical properties and the kinetics of the oxygen reactions of the advanced SS mesh electrode are performed by electrochemical impedance spectroscopy (EIS) (**Figure 3**). A typical Nyquist plot of a single-cell practical zinc-air battery is composed of two semicircles that correspond to different battery processes well-described by an equivalent circuit with five elements, solution resistance (R_s), solid-electrolyte interface resistance (R_{int}), charge transfer resistance (R_{ct}), and constant phase elements (Q_{int} and Q_{dl}) (Figure 3, inset).[2,22] The values of these elements for each electrode investigated are listed in **Table 1**. The advanced SS mesh electrode shows significantly lower values for all three resistances, which again highlights the advantages of the hierarchical design of the air electrode. The lowest R_s value of the advanced SS electrode is attributed to the reduction

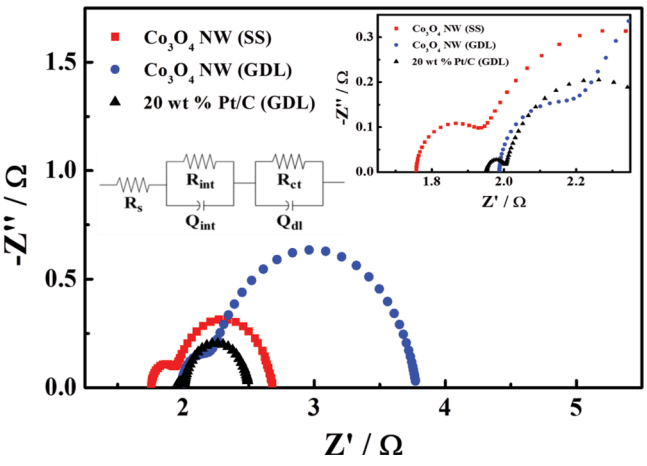

Figure 3. Nyquist plots obtained by EIS using air under ambient conditions of Co_3O_4 NWs grown on SS mesh (red square), Co_3O_4 NWs sprayed on GDL (blue circle), and Pt/C sprayed on GDL (black triangle). Inset: High frequency range of the Nyquist plot, and the equivalent circuit.

Table 1. The values of the equivalent circuit elements based on the EIS analysis of Co_3O_4 NWs grown on SS mesh, Co_3O_4 sprayed on GDL, and Pt/C sprayed on GDL.

Element	Co_3O_4 NWs grown on SS mesh	Co_3O_4 NWs sprayed on GDL	20 wt% Pt/C sprayed on GDL
R_s [Ω]	1.76	1.987	2.05
R_{int} [Ω]	0.179	0.209	0.050
R_{ct} [Ω]	0.744	1.58	0.498
Q_{int} [S s^n]	0.0378	0.0155	0.207
Q_{dl} [S s^n]	1.49×10^{-3}	9.73×10^{-4}	2.55×10^{-3}

of the internal resistance by directly coupling the active Co_3O_4 NW array onto the current collector and reducing the battery components required. In comparison, the conventional GDL electrode sprayed with Co_3O_4 NWs exhibits much larger R_s likely due to randomly oriented NW (no longer individually self-standing) with possible particle aggregation. R_{int} of the advance electrode is also much lower than that of the conventional electrodes as the interfacing of the NW array with electrolyte is much easier in the self-standing geometry and without the interference from the polymer binder. In addition, the advanced electrode exhibits a very reduced R_{ct} compared to that of the conventional electrode, which is attributed to enhanced transfer of charges and greater active material utilization during the electrochemical reaction.

Building upon the demonstration of high functionality of the advanced electrode, its practicality is demonstrated by investigating the long term durability using the extended cycling test (3 h discharge followed by 3 h charge) in a practical zinc-air battery. The advanced SS electrode with directly coupled Co_3O_4 NWs demonstrates excellent charge and discharge potentials, consistent with the pulse cycling (**Figure 4**a). The discharge profiles show a shallow linear potential drop over the duration of the 3 h battery discharge, which is attributed to the gradual exhaustion of the hydroxide ions in the electrolyte during ORR, not due to the degradation in the performance of the electrode. The lack of hydroxide ions in the electrolyte can be simply refuelled in practice by utilizing a flow electrolyte battery design. The extended cycling of the advanced SS electrode shows remarkable charge and discharge potential retentions (97% and 94%, respectively) even after 100 cycles (nearly a month). The durability of a zinc-air battery with such excellent rechargeable potentials over this time-scale has not been previously reported (Supporting Information Figure S9). In comparison, the conventional GDL electrode demonstrates very poor rechargeability, lasting only four cycles (Figure 4b). The peaks observed in the charge profiles of the conventional electrode, which are absent in those of the SS mesh electrode, are attributed to the carbon corrosion of the GDL and the polymer binder at higher charge potentials. This highly undesirable reactions lead to the physical degradation of the air cathode, significantly reducing the rechargeability of the zinc-air battery. The detrimental effect of using the conventional GDL is also observed with Pt/C sprayed electrode, where a significantly limited rechargeability of only four cycles is observed (Figure 4c).

In summary, we propose an advanced air electrode with functionality and practicality for long term rechargeable zinc-air battery applications. The electrode is composed of a hierarchical self-standing mesoporous Co_3O_4 NW array as a highly active bifunctional catalyst for both ORR and OER. The Co_3O_4 NW array is directly coupled to the underlying SS mesh current collector via a facile synthesis, which does not require the use of any ancillary material. The advanced electrode preparation also eliminates conventionally used physical deposition processes such as spray-coating or drop-casting. Compared to the conventional GDL electrodes, the advanced electrode exhibits superior charge and discharge potentials at high currents. Furthermore, 1500 pulse cycles are demonstrated without significant performance degradation, exhibiting excellent rechargeability. In addition, superior internal, interfacial,

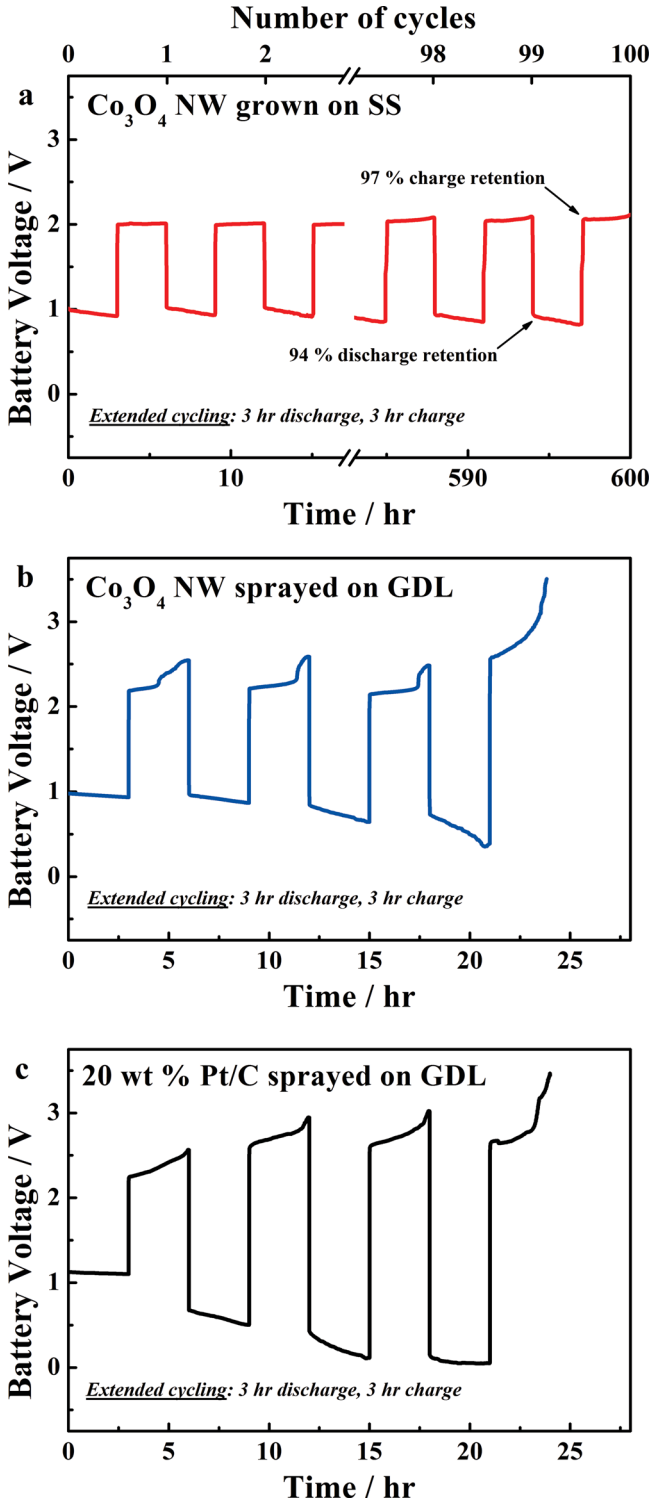

Figure 4. The extended practical zinc-air battery cycling tests using air under ambient conditions of a) Co_3O_4 NWs grown on SS mesh, b) Co_3O_4 NWs sprayed on GDL, and c) Pt/C sprayed on GDL.

and charge transfer resistances of the advanced electrode have been confirmed by EIS, attributed to the advantages of directly coupling Co_3O_4 NW onto the current collector. Finally,

remarkable electrochemical durability of the advanced electrode is observed utilizing air in ambient conditions, demonstrating extended cycling of 600 h with charge and discharge potential retentions of 97% and 94%, respectively. This excellent longevity of the advanced electrode is attributed to the directly coupled Co_3O_4 NW array on the SS mesh, which remains intact and highly active even after extremely long battery operation.

Experimental Section

The single-cell battery performance was tested using a home-made practical zinc-air battery and a multichannel potentiostat (Princeton Applied Research, VersaSTAT MC). A polished zinc plate (Zinc Sheet EN 988, OnlineMetals) and Co_3O_4 NWs directly grown on SS mesh (Super fine #500 E-Cig 25 µm, The Mesh Company) were used as the anode and cathode, respectively. A Teflon-coated carbon fiber paper as a backing layer was placed next to the SS mesh to prevent electrolyte leakage. A microporous membrane (25 µm polypropylene membrane, Celgard 5550) and 6.0 M KOH were used as the separator and electrolyte, respectively. The area of the active material layer exposed to the electrolyte was 2.84 cm^2. For comparison, cathodes consisting of Co_3O_4 NWs (scrapped off from the SS mesh) and 20 wt% commercial Pt/C were spray-coated using an air brush onto a GDL with a loading of ca. 1.5 mg cm^{-2}, consistent with the average loading of Co_3O_4 NW directly grown on SS mesh. Briefly, 15 mg of active material was dispersed in 1 mL of isopropyl alcohol by sonication for 30 min. 107 µL of 5 wt% Nafion solution was added followed by 1 h of additional sonication. The catalyst mixture was sprayed onto the GDL then dried in an oven at 60 °C for 1 h. The catalyst loading was determined by measuring the weight of the GDL before and after spray-coating. The discharge and charge polarization and power density plots were obtained using a galvanodynamic method with a current density ranging from 0 to 200 mA. The charge-discharge pulse cycling was conducted by a recurrent galvanic pulse method with a fixed current of 50 mA with each cycle being 10 min (5 min discharge followed by 5 min charge). The extended cycling was carried out using the same method but with each cycle lasting 6 h (3 h discharge followed by 3 h charge). The zinc plate was replaced every 20 cycles to study the durability of air cathode without the failure of battery due to the anode. Electrochemical impedance spectroscopy was conducted with a direct current (DC) voltage fixed at an ORR potential of 0.8 V with an alternating current (AC) voltage of 20 mV ranging from 100 kHz to 0.1 Hz to obtain the Nyquist plots.

Supporting Information

Supporting Information is available from the Wiley Online Library or from the author.

Acknowledgements

This research was supported by the Natural Sciences and Engineering Research Council of Canada (NSERC) through grants to Z.C. and the University of Waterloo.

Received: September 11, 2013
Revised: October 12, 2013
Published online: December 4, 2013

[1] G. Girishkumar, B. McCloskey, A. C. Luntz, S. Swanson, W. Wilcke, *J. Phys. Chem. Lett.* **2010**, *1*, 2193.
[2] Z. Chen, A. Yu, D. Higgins, H. Li, H. Wang, Z. Chen, *Nano Lett.* **2012**, *12*, 1946.
[3] J. Chen, F. Y. Cheng, *Acc. Chem. Res.* **2009**, *42*, 713.
[4] H. W. Park, D. U. Lee, L. F. Nazar, Z. Chen, *J. Electrochem. Soc.* **2013**, *160*, A344.
[5] J. Wu, H. W. Park, A. Yu, D. Higgins, Z. Chen, *J. Phys. Chem. C* **2012**, *116*, 9427.
[6] Z. Chen, J. Y. Choi, H. J. Wang, H. Li, Z. W. Chen, *J. Power Sources* **2011**, *196*, 3673.
[7] J. S. Lee, G. S. Park, H. I. Lee, S. T. Kim, R. G. Cao, M. L. Liu, J. Cho, *Nano Lett.* **2011**, *11*, 5362.
[8] V. Neburchilov, H. J. Wang, J. J. Martin, W. Qu, *J. Power Sources* **2010**, *195*, 1271.
[9] Z. Chen, M. Waje, W. Li, Y. Yan, *Angew. Chem.* **2007**, *119*, 4138.
[10] T. Ioroi, N. Kitazawa, K. Yasuda, Y. Yamamoto, H. Takenaka, *J. Electrochem. Soc.* **2000**, *147*, 2018.
[11] T. Yu, D. Y. Kim, H. Zhang, Y. Xia, *Angew. Chem. Int. Ed.* **2011**, *50*, 2773.
[12] D. C. Higgins, S. Y. Ye, S. Knights, Z. W. Chen, *Electrochem. Solid State Lett.* **2012**, *15*, B83.
[13] K. P. Gong, F. Du, Z. H. Xia, M. Durstock, L. M. Dai, *Science* **2009**, *323*, 760.
[14] Y. Liang, Y. Li, H. Wang, H. Dai, *J. Am. Chem. Soc.* **2013**, *135*, 2013.
[15] Y. Li, M. Gong, Y. Liang, J. Feng, J.-E. Kim, H. Wang, G. Hong, B. Zhang, H. Dai, *Nat. Commun.* **2013**, *4*, 1805.
[16] K. H. Kangasniemi, D. A. Condit, T. D. Jarvi, *J. Electrochem. Soc.* **2004**, *151*, E125.
[17] X. Wang, W. Z. Li, Z. W. Chen, M. Waje, Y. S. Yan, *J. Power Sources* **2006**, *158*, 154.
[18] Y. G. Li, B. Tan, Y. Y. Wu, *Nano Lett.* **2008**, *8*, 265.
[19] Y. D. Yin, R. M. Rioux, C. K. Erdonmez, S. Hughes, G. A. Somorjai, A. P. Alivisatos, *Science* **2004**, *304*, 711.
[20] Y. Y. Gao, S. L. Chen, D. X. Cao, G. L. Wang, J. L. Yin, *J. Power Sources* **2010**, *195*, 1757.
[21] G. Binotto, D. Larcher, A. S. Prakash, R. H. Urbina, M. S. Hegde, J. M. Tarascon, *Chem. Mater.* **2007**, *19*, 3032.
[22] D. Thiele, A. Züttel, *J. Power Sources* **2008**, *183*, 590.

